Meteoritics & Planetary Science 37, 533–548 (2002)
Available online at http://www.uark.edu/meteor

A hibonite-corundum inclusion from Murchison: A first-generation condensate from the solar nebula

S. B. SIMON[1]*, A. M. DAVIS[1,2], L. GROSSMAN[1,2] AND K. D. MCKEEGAN[3]

[1]Department of the Geophysical Sciences, The University of Chicago, 5734 South Ellis Avenue, Chicago, Illinois 60637, USA
[2]Enrico Fermi Institute, The University of Chicago, 5640 South Ellis Avenue, Chicago, Illinois 60637, USA
[3]Department of Earth and Space Sciences, University of California, Los Angeles, California 90095, USA
*Correspondence author's e-mail address: sbs8@midway.uchicago.edu

(Received 2001 May 21; accepted in revised form 2001 December 21)

Abstract–Through freeze-thaw disaggregation of the Murchison (CM) carbonaceous chondrite, we have recovered a ~90 × 75 μm refractory inclusion that consists of corundum and hibonite with minor perovskite. Corundum occurs as small (~10 μm), rounded grains enclosed in hibonite laths (~10 μm wide and 30–40 μm long) throughout the inclusion. Perovskite predominantly occurs near the edge of the inclusion. The crystallization sequence inferred petrographically—corundum followed by hibonite followed by perovskite—is that predicted for the first phases to form by equilibrium condensation from a solar gas for $P^{tot} \leq 5 \times 10^{-3}$ atm. In addition, the texture of the inclusion, with angular voids between subhedral hibonite laths and plates, is also consistent with formation of the inclusion by condensation. Hibonite has heavy rare earth element (REE) abundances of ~40 × CI chondrites, light REE abundances ~20 × CI chondrites, and negative Eu anomalies. The chondrite-normalized abundance patterns, especially one for a hibonite-perovskite spot, are quite similar to the patterns of calculated solid/gas partition coefficients for hibonite and perovskite at 10^{-3} atm and are not consistent with formation of the inclusion by closed-system fractional crystallization. In contrast with the features that are consistent with a condensation origin, there are problems with any model for the formation of this inclusion that includes a molten stage, relic grains, or volatilization. If thermodynamic models of equilibrium condensation are correct, then this inclusion formed at pressures $<5 \times 10^{-3}$ atm, possibly with enrichments (<1000×) in CI dust relative to gas at low pressures (below 10^{-4} atm). Both hibonite and corundum have $\delta^{17}O \approx \delta^{18}O \approx -50‰$, indicating formation from an ^{16}O-rich source. The inclusion does not contain radiogenic ^{26}Mg and apparently did not contain live ^{26}Al when it formed. If the short-lived radionuclides were formed in a supernova and injected into the early solar nebula, models of this process suggest that ^{26}Al-free refractory inclusions such as this one formed within the first ~6×10^5 years of nebular collapse.

INTRODUCTION

Equilibrium thermodynamic condensation calculations for a cooling solar gas at $P^{tot} < 10^{-2}$ atm (*e.g.*, Yoneda and Grossman, 1995) show that corundum should be the first major condensate. With continued cooling, corundum is predicted to react with the nebular vapor to form hibonite. Apparently, in many cases it did so, because hibonite-bearing inclusions are much more abundant than corundum-bearing ones in carbonaceous chondrites. Inclusions containing possible primary corundum and hibonite have been reported by Bar-Matthews *et al.* (1982), Fahey (1988) and by Krot *et al.* (2001). In their study of BB-5, the first corundum-bearing inclusion ever reported, Bar-Matthews *et al.* (1982) favored a condensation origin over an igneous one, but could not draw a firm conclusion because (a) they could not tell from the texture of the sample whether it crystallized from a melt or was a direct gas-solid condensate, and (b) adequate thermodynamic data for hibonite were not yet available. It was not known whether hibonite should condense from a gas of solar composition, and, if so, whether it should do so before or after corundum. The corundum in another inclusion, GR-1, most likely formed by the partial breakdown of hibonite (MacPherson *et al.*, 1984; Hinton *et al.*, 1988). Hibonite, being the most refractory major phase that is a carrier of rare earth elements (REE), and commonly containing isotopic anomalies (*e.g.*, Ireland *et al.*, 1991), can yield important insights into physico-chemical conditions in the early solar nebula.

The Murchison inclusion described herein appears to contain primary corundum enclosed in hibonite. With the

Prelude preprint MS#4555

scanning electron microscope, electron microprobe and ion microprobe, we have conducted a detailed study of this object in order to gain insights into the early history of the solar system. Pristine, unmelted inclusions are especially important in light of the growing number of studies (*e.g.*, MacPherson and Davis, 1993; Beckett *et al.*, 2000; Grossman *et al.*, 2000) that provide strong evidence that many refractory inclusions, especially type B inclusions, have undergone complex thermal histories involving, for example, multiple melting events and probably evaporation. Such events can overprint the chemical and isotopic information recorded earliest in the inclusions, whereas unmelted condensate assemblages potentially provide direct information about possible pressures, temperatures, and isotopic compositions in the early solar nebula. Preliminary results of this study were reported by Simon *et al.* (2000a).

ANALYTICAL METHODS

The sample, M98-8, was recovered by hand-picking from the high-density ($\rho > 3.2$) separate obtained from the products of freeze-thaw disaggregation of a bulk sample of Murchison by the method of MacPherson *et al.* (1980). Backscattered electron images and x-ray maps of a polished thin section of the sample were obtained with a JEOL JSM-5800LV scanning electron microscope equipped with an Oxford/Link ISIS-300 energy-dispersive x-ray microanalysis system. Quantitative wavelength-dispersive analyses were obtained with a Cameca SX-50 electron microprobe operated at 15 kV with a beam current of 25 nA. Data were reduced *via* the modified ZAF correction procedure PAP (Pouchou and Pichoir, 1984). Trace element and Mg isotopic analyses were obtained using the University of Chicago AEI IM-20 ion microprobe. The analytical techniques used are similar to those described in Simon *et al.* (1991), MacPherson and Davis (1993, 1994) and Russell *et al.* (2000). Trace element analyses were done using energy filtering. A variety of silicate standards were used to determine calcium-normalized yields. NIST 611 glass was analyzed at the beginning and end of the run to correct for variations in ion yield that are a function of mass (MacPherson and Davis, 1994). For Mg isotopic analyses, Madagascar hibonite was used as a standard for determining instrumental mass fractionation.

After cleaning and recoating of the sample, oxygen isotopic abundances were determined with the UCLA CAMECA ims 1270 ion microprobe utilizing techniques similar to those described in Simon *et al.* (2000b). A Cs primary ion beam was used to sputter shallow, elliptically-shaped craters of ~12 × 18 μm. Analyses were performed without energy filtering at high mass resolving power using an electron flood gun for achieving charge compensation. Sample topography and previous ion probe analyses limited the surface area available for oxygen isotope measurements and contributed to slightly larger errors of 2 to 3‰ (1σ) for $\delta^{18}O$ and $\delta^{17}O$ in each of three spots analyzed.

RESULTS

Petrography

The sample appeared pale green prior to sectioning but is colorless in thin section. A backscattered electron image of M98-8 (Fig. 1) shows that it is rounded, and ~90 × 75 μm. It is dominated by subhedral hibonite laths that are mostly ~10 μm wide and 30–40 μm long. Most hibonite laths enclose rounded, anhedral grains of corundum that are 5 μm across. The largest corundum grain is ~15 μm in size. Small grains of perovskite, a few microns across, are also present, mostly occurring at the edges of hibonite grains and at the edge of the inclusion. Small grains of Mg-Fe phyllosilicate, a secondary phase that is common in Murchison, are found predominantly at the edge of the inclusion, but also in some of the interior cavities. Elemental x-ray maps (Fig. 2) help illustrate the distribution of phases. The phyllosilicate is the bright phase in the Si map, and perovskite is bright in the Ca and Ti maps. Corundum is bright in the Al map and black in the Ca map. From counting 5870 points (excluding the voids) on the backscattered electron image, we obtained a mode of 89.1 vol% hibonite, 9.3% corundum, and 1.6% perovskite.

There is void space between many of the hibonite grains, giving the object a somewhat fluffy texture. Many of these voids, their shapes controlled by hibonite crystals, are triangular- or trapezoidal-shaped gaps between laths, like those shown in Fig. 3. In some of the voids, hibonite crystal faces can be seen jutting into open space, and some contain unpolished plates below the surface of the section (Fig. 3b). The textures of two corundum-bearing inclusions from Adelaide can also be described as fluffy. They were found *in situ* (Krot *et al.*, 2001), and meteorite matrix or rim material occurs between many of the hibonite crystals. The overall texture of M98-8 is different from those of the two other hibonite-corundum inclusions that have been found in Murchison, BB-5 (Bar-Matthews *et al.*, 1982) and GR-1 (MacPherson *et al.*, 1984). Sample BB-5 is more compact than M98-8 and its corundum is subhedral and concentrated in the core of the inclusion, rather than dispersed throughout the inclusion as in M98-8. Sample GR-1 has a euhedral hibonite crystal at its core. This grain is enclosed in corundum, and hibonite is also present at the edge of the inclusion. Murray sample F5 (Fahey, 1988) is similar to the Adelaide inclusions in that it consists of hibonite laths that enclose small corundum grains and appears to be very loosely consolidated, with meteorite matrix between hibonite grains.

Mineral Chemistry

Corundum compositions are nearly pure Al_2O_3, as shown by the representative analyses given in Table 1. Small amounts of TiO_2 are also present, as is the case for BB-5 (Bar-Matthews *et al.*, 1982) and GR-1 (MacPherson *et al.*, 1984). Corundum

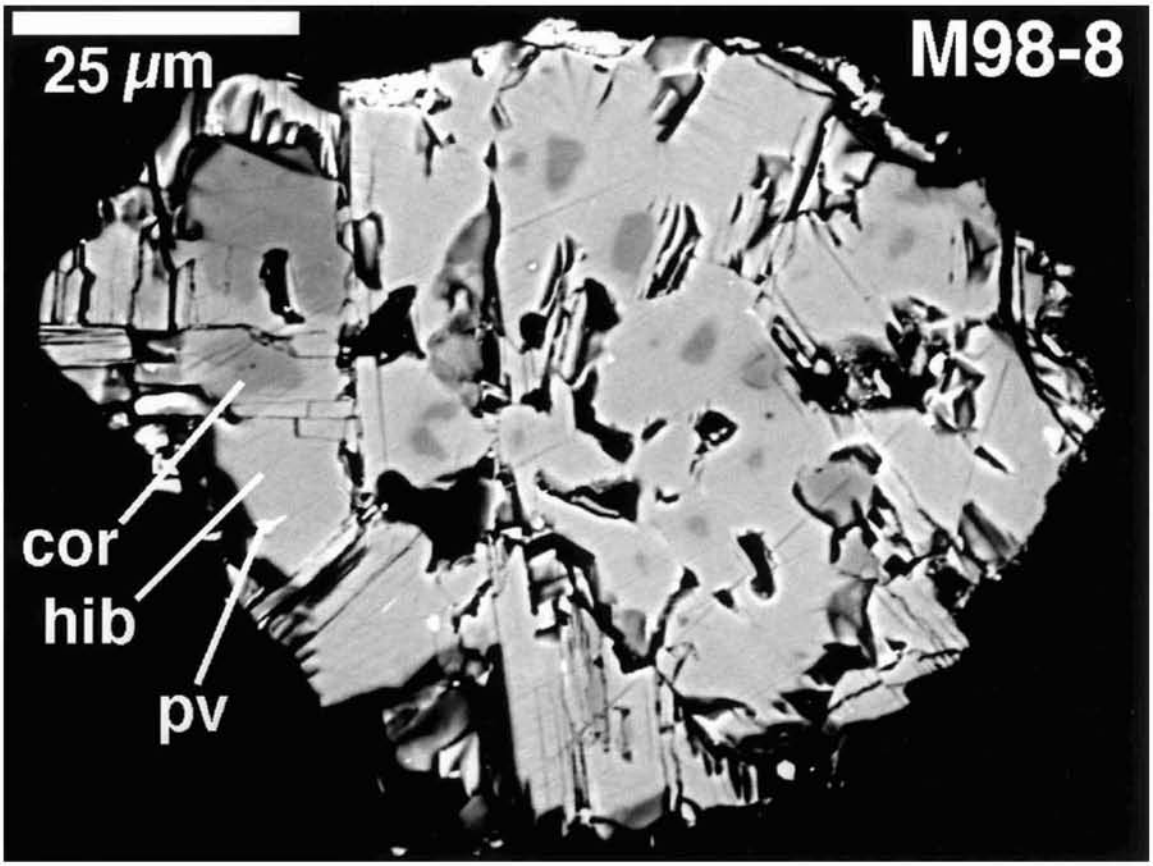

FIG. 1. Backscattered electron image of M98-8. Corundum is the dark gray phase seen at the upper left and as isolated, rounded grains enclosed in hibonite (light gray). Void spaces and epoxy are black. cor = corundum; hib = hibonite; pv = perovskite.

TABLE 1. Electron microprobe analyses of corundum in M98-8.

	1	2
Al_2O_3	99.85	99.61
SiO_2	0.02	BDL
CaO	0.09	0.05
TiO_2	0.17	0.25
FeO	BDL	0.04
Total	100.13	99.95
Cations per 3 oxygen anions		
Al	1.995	1.995
Si	0	0
Ca	0.002	0.001
Ti	0.002	0.003
Fe	0	0.001
Total cations	1.999	2.000

BDL = below detection limit (in wt%) of 0.012 for SiO_2; or 0.036 for FeO. Also below detection: MgO (<0.015 wt%); Sc_2O_3 (<0.032); and V_2O_3 (<0.027).

in F5 contains <0.1 wt% TiO_2 (Fahey, 1988). In the M98-8 corundum, as in the other occurrences, abundances of MgO, Sc_2O_3, and V_2O_3 are all below the detection limits of the electron microprobe.

Representative compositions of hibonite from M98-8 are given in Table 2. The crystals are not zoned, and all contain <2 wt% TiO_2. The overall range in TiO_2 contents is from 1.2 to 1.9 wt%, and most grains have between 1.5 and 1.9 wt%. Abundances of Sc_2O_3, V_2O_3, FeO and, in most cases, SiO_2 are below the detection limits of the electron probe. Hibonite in the other corundum-bearing inclusions also has TiO_2 contents $\leq$2 wt%. The large, single crystals of hibonite found in Murchison also tend to have low TiO_2 contents, while the hibonite from spinel-hibonite spherules typically has 3–7 wt% TiO_2 (Ireland, 1988). Trivalent Ti can substitute for Al in hibonite, and tetravalent Ti and Si cations can enter hibonite along with Mg *via* a coupled substitution for two Al^{3+} cations. If Ti^{3+} proportions are negligible, a plot of Mg *vs.* Ti + Si cation abundances in meteoritic hibonite typically yields a trend with a slope of 1. Such a line, shown for reference in Fig. 4, passes through the data, with most points on or close to the line, suggesting that Ti^{3+} proportions are low. If Ti^{3+} contents were significant, the data would plot on the high-Ti

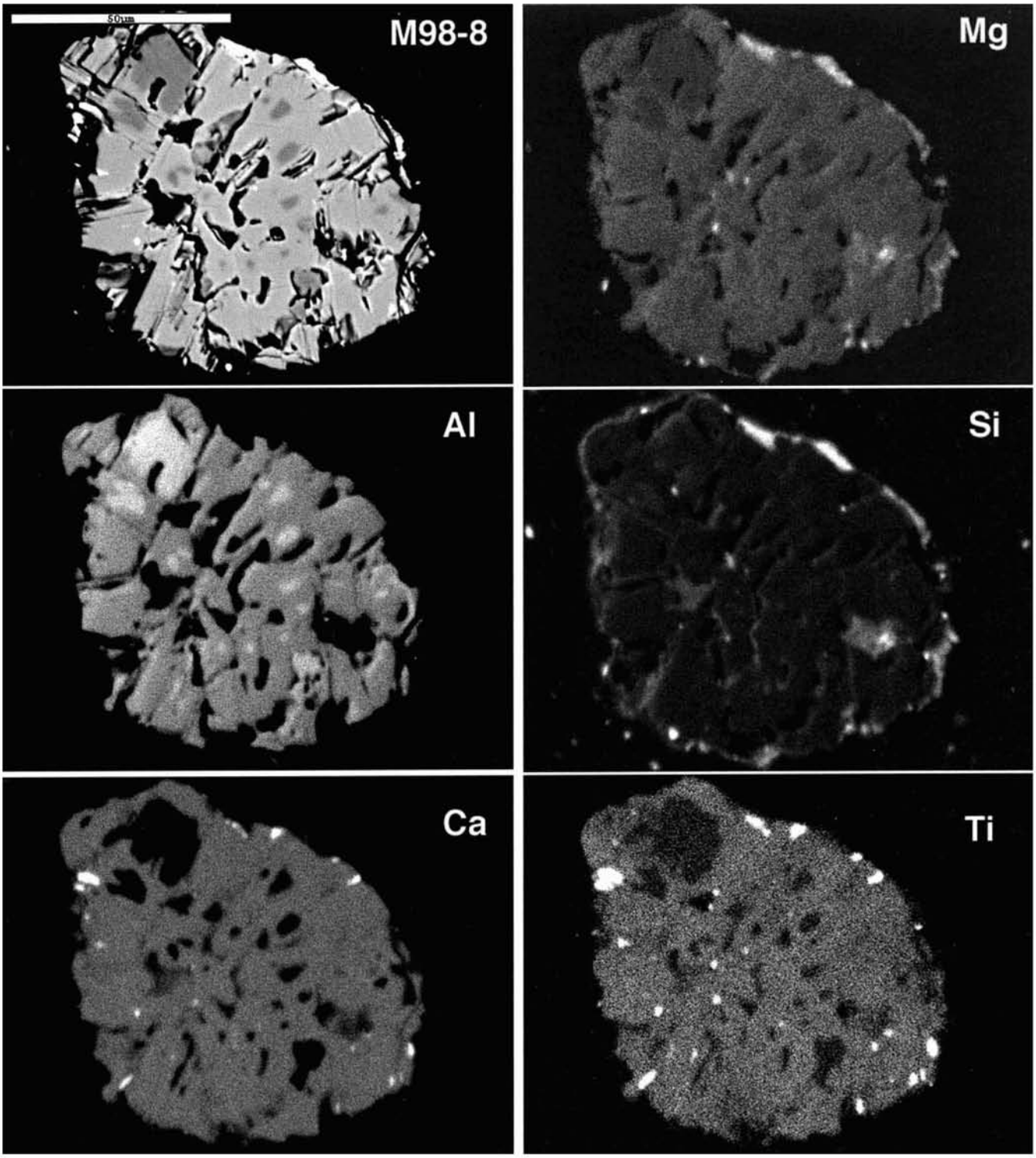

FIG. 2. Backscattered electron image (upper left) and elemental x-ray maps of M98-8. Note the distribution of corundum (bright in Al map) throughout the inclusion, and the tendency of perovskite (bright in Ca and Ti maps) and phyllosilicate (bright in Si map) to occur at the edge of the inclusion.

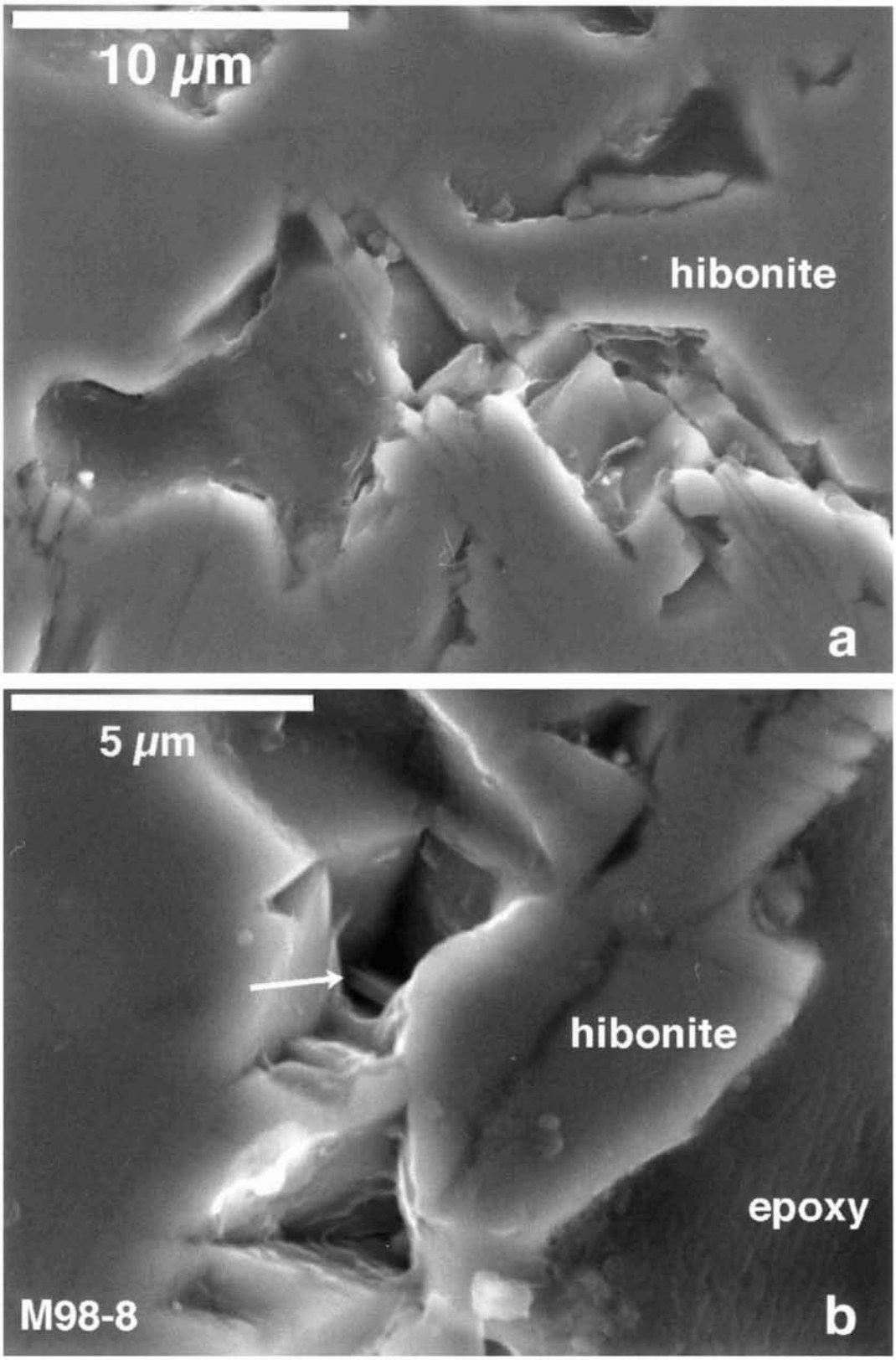

FIG. 3. Secondary electron images of M98-8 showing void space bounded by crystal faces (*e.g.*, upper right in both (a) and (b)) and unpolished plates below the surface of the section (arrow near center of (b)).

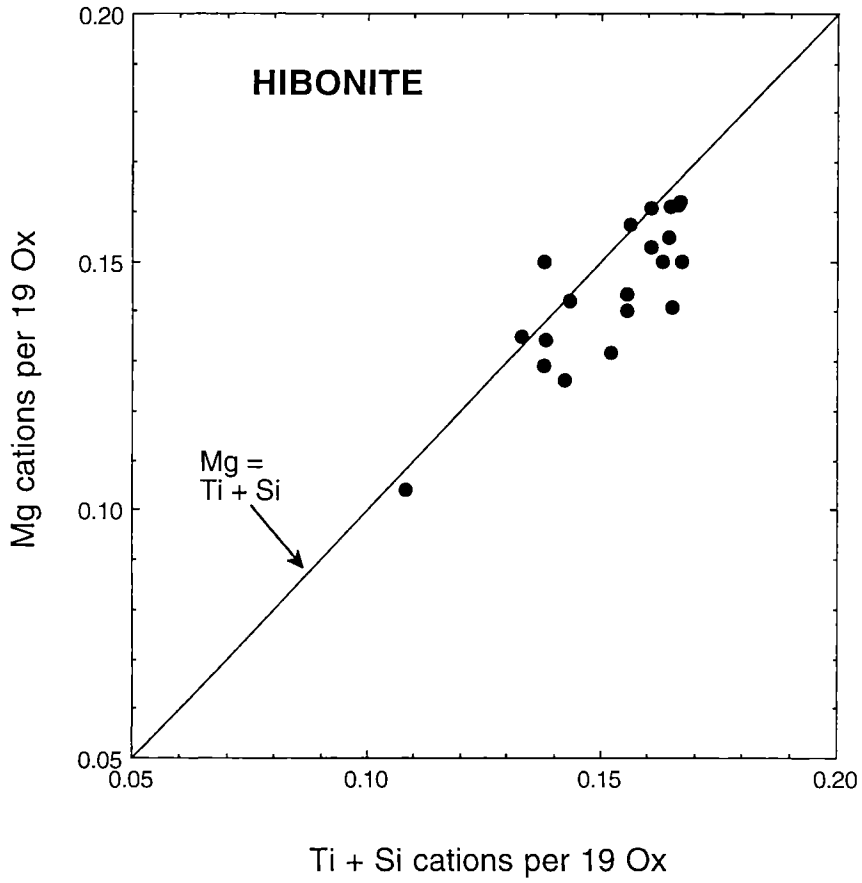

FIG. 4. Electron microprobe analyses of hibonite in M98-8. The hibonite has low TiO_2 contents and the data scatter about the 1:1 correlation line for Mg *vs.* Ti + Si cations, which is shown for reference.

TABLE 2. Electron microprobe analyses of hibonite in M98-8.

	1	2	3
MgO	0.81	0.98	0.90
Al_2O_3	88.96	88.86	88.61
SiO_2	BDL	0.08	BDL
CaO	8.59	8.59	8.42
TiO_2	1.64	1.88	1.92
Total	100.00	100.39	99.85
	Cations per 19 oxygen anions		
Mg	0.134	0.162	0.150
Al	11.706	11.651	11.676
Si	0	0.009	0
Ca	1.028	1.024	1.009
Ti	0.138	0.158	0.161
Total cations	13.006	13.004	12.996

BDL = below detection limit of 0.012 wt%. Also below detection: Sc_2O_3 (<0.042 wt%); V_2O_3 (<0.033); and FeO (<0.039).

side of the slope-1 line and further from it with increasing Ti content.

Trace Element Abundances

Ion microprobe analyses are given in Table 3, and chondrite-normalized REE abundance patterns are illustrated in Fig. 5. All of the spots are hibonite-dominated, though one spot sampled perovskite (probably ~4 wt%, based on the TiO_2 content) and Mg-, Fe-silicate in addition to hibonite. The other two spots have rather similar trace element concentrations to each other, so they were averaged for Fig. 5. The patterns have some features in common, and some differences. Each of the analyses has (chondrite-normalized) heavy REE (HREE) > light REE (LREE), as found in ultrarefractory inclusions, although the HREE enrichment relative to the LREE in M98-8 is not as pronounced as it is in most ultrarefractory inclusions. The pattern for the perovskite-poor analysis has flat LREE abundances as does the perovskite-rich analysis, except that abundances decrease from Nd through Eu in the latter. The chondrite-normalized HREE patterns are different from each other and are unusual in that Tm is enriched relative to Er in

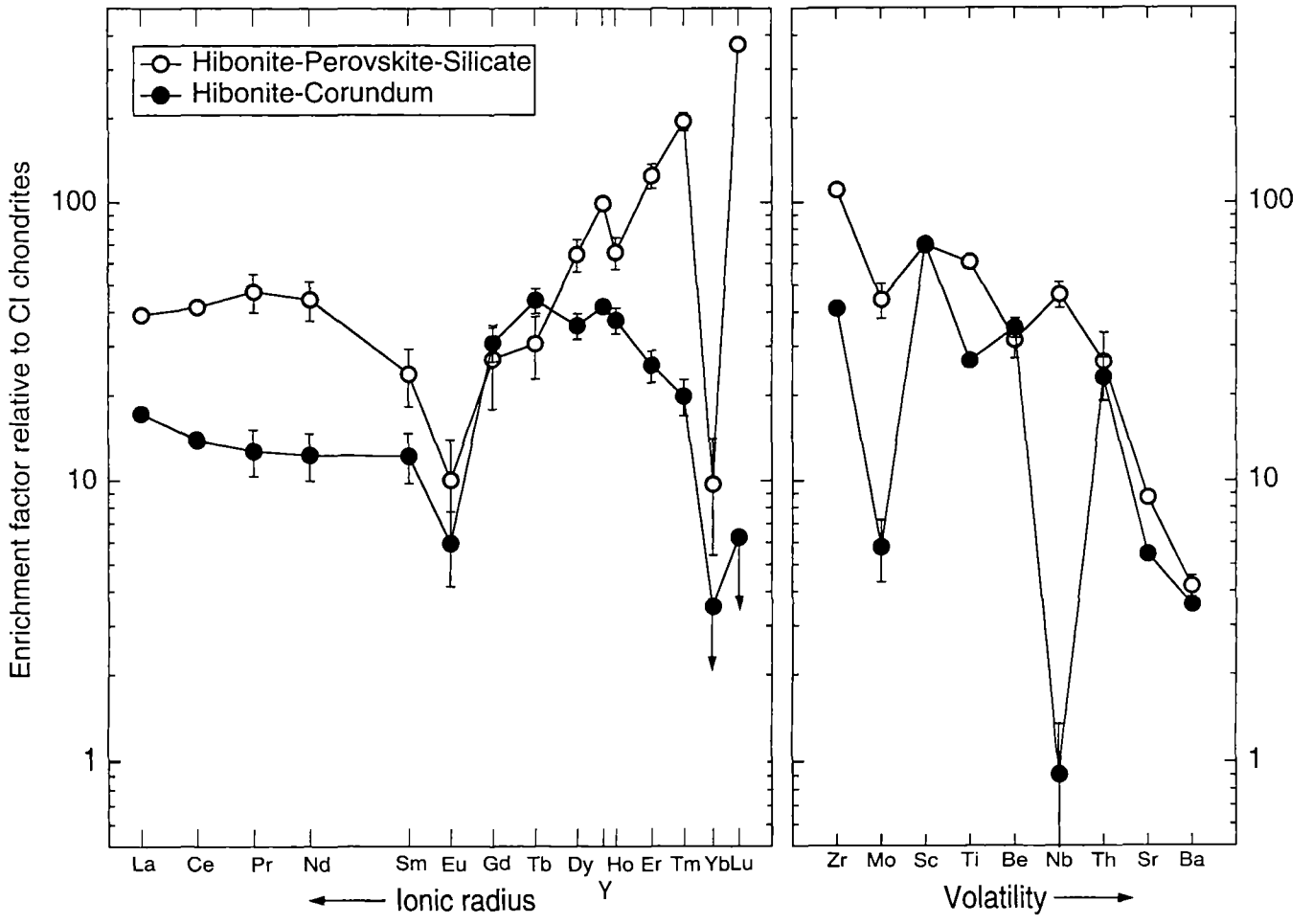

FIG. 5. Chondrite-normalized rare earth element and refractory trace element abundances in M98-8, measured by ion microprobe. The enrichment of heavy REE relative to light REE is characteristic of ultrarefractory inclusions.

one analysis and enriched relative to Lu in the other, whereas in most ultrarefractory inclusions Tm is significantly depleted relative to both Er and Lu. The hibonite-corundum pattern, in which Tb, Dy, Y and Ho have the greatest enrichment factors with a "roll-off" through the heavier REE resembles the hibonite + perovskite pattern reported for BB-5 (Hinton *et al.*, 1988). In contrast, the Murray inclusion F5 has a group II REE pattern (Fahey, 1988). Among other trace elements, the hibonite in M98-8 contains ~400 ppm Sc and 120–350 ppm Zr, and these values are within the range of those reported for Murchison hibonite by Ireland *et al.* (1988). The CI-normalized refractory trace element abundance pattern for the perovskite-poor analysis is similar to that for the perovskite-rich one, except that the former is depleted in Mo and Nb relative to the latter (Fig. 5). This is not surprising, as perovskite is typically Nb-rich (Ireland *et al.*, 1988).

Isotopic Abundances

Measurements of the intrinsic mass-fractionation of magnesium, F_{Mg}, are all within 2σ error of –5‰, and three of the five analyses are within error of 0‰ (Table 4). Neither the hibonite nor the corundum incorporated measurable live ^{26}Al when they formed. On a plot of $\delta^{26}Mg$ *vs.* $^{27}Al/^{24}Mg$ (Fig. 6), the best-fit line through the data has a negative slope, but all the measurements of $\delta^{26}Mg$ are within error of 0. Many calcium-aluminum-rich inclusions (CAIs) consist of phases with excess ^{26}Mg abundances that are consistent with initial $^{26}Al/^{27}Al$ ratios of ~5×10^{-5} (*e.g.*, MacPherson *et al.*, 1995). In contrast, the upper limit for the initial $^{26}Al/^{27}Al$ ratio of the present sample, based on the 2σ upper limit on the slope of the line through the data points, is ~1.6×10^{-6}. No evidence of live ^{26}Al was found in BB-5 (Bar-Matthews *et al.*, 1982), while Fahey (1988) reported an initial $^{26}Al/^{27}Al$ ratio of $(4.1 \pm 0.2) \times 10^{-5}$ for F5.

Oxygen isotopic compositions in M98-8 were determined in two spots of pure hibonite, while spot three sampled a mixture of hibonite and corundum (Table 5). We do not know precisely the corundum/hibonite ratio of the analytical volume, but inspection of the spot three pit after analysis indicates that it apparently contained at least 50% hibonite. As the composition of the corundum + hibonite spot is within error of the hibonite analyses, the isotopic composition of the corundum is probably

TABLE 3. Major and trace element abundances in three analysis spots on Murchison M98-8, determined by ion microprobe.*

	#6	#7	#8
Phase†	hib-cor	hib-pv-sil	hib-cor
MgO	0.701	1.39	0.766
Al_2O_3	87.2	72.6	88.0
SiO_2	0.243	10.1	0.527
CaO	9.58	9.02	8.28
TiO_2	1.97	4.32	1.81
FeO	0.213	1.27	0.440
Li	0.254 ± 0.054	0.85 ± 0.12	0.200 ± 0.051
Be	0.848 ± 0.095	0.78 ± 0.11	0.87 ± 0.10
B	0.72 ± 0.18	5.10 ± 0.58	1.55 ± 0.29
Na	45.7	5930	104
P	5.4 ± 3.9	<36	11.7 ± 6.0
K	11.6 ± 1.3	341	24.9 ± 2.3
Sc	393	424	461
V	70.1 ± 5.2	68.8 ± 7.6	63.3 ± 5.6
Cr	5.7 ± 2.0	149 ± 9	44.5 ± 4.6
Mn	9.0 ± 1.6	27 ± 14	15.4 ± 2.5
Co	4.6 ± 2.2	40.6 ± 7.3	7.0 ± 2.9
Ni	97 ± 16	896 ± 55	185 ± 25
Rb	0.34 ± 0.25	2.19 ± 0.75	0.35 ± 0.26
Sr	38.1	67.0	46.0
Y	71.6	151	55.6
Zr	138	351	123
Nb	0.088 ± 0.083	10.4 ± 1.1	0.32 ± 0.18
Mo	2.4 ± 1.1	39.8 ± 5.8	8.0 ± 2.3
Ba	8.35 ± 0.64	9.60 ± 0.86	8.09 ± 0.70
La	3.44 ± 0.25	9.16 ± 0.50	4.66 ± 0.32
Ce	6.19 ± 0.54	25.1 ± 1.3	10.6 ± 0.8
Pr	1.21 ± 0.29	4.22 ± 0.66	1.06 ± 0.30
Nd	6.8 ± 1.6	20.1 ± 3.3	4.3 ± 1.4
Sm	1.89 ± 0.50	3.51 ± 0.82	1.70 ± 0.51
Eu	0.27 ± 0.13	0.56 ± 0.22	0.40 ± 0.15
Gd	5.7 ± 1.2	5.3 ± 1.8	6.4 ± 1.3
Tb	1.54 ± 0.22	1.11 ± 0.28	1.66 ± 0.25
Dy	11.1 ± 1.4	15.7 ± 2.1	6.2 ± 1.2
Ho	2.31 ± 0.31	3.66 ± 0.49	1.84 ± 0.31
Er	5.24 ± 0.83	19.8 ± 2.0	2.91 ± 0.68
Tm	0.62 ± 0.11	4.71 ± 0.36	0.338 ± 0.090
Yb	0.48 ± 0.43	1.58 ± 0.70	<0.76
Lu	<0.20	8.98 ± 0.51	<0.22
Th	0.56 ± 0.15	0.77 ± 0.21	0.80 ± 0.19
U	0.115 ± 0.066	<0.11	<0.089

*Oxide concentrations are given in wt% and elemental concentrations in ppm. Uncertainties are $\pm 1\sigma$, based on counting statistics, and are only given where they exceed 5% of the amount present; upper limits are $<2\sigma$.

†Abbreviations: hib = hibonite; cor = corundum; sil = Mg, Fe-rich silicate.

TABLE 4. $^{27}Al/^{24}Mg$ ratios and Mg isotopic compositions of M98-8.

	$^{27}Al/^{24}Mg$	F_{Mg} (‰/amu)	$\delta^{26}Mg$ (‰)
hib	113.6 ± 8.1	−10.2 ± 4.7	2.6 ± 6.8
hib	168.6 ± 3.3	−6.5 ± 3.3	−0.4 ± 5.0
hib	215 ± 27	−3.0 ± 3.8	−1.6 ± 4.9
hib	80.9 ± 0.6	−2.8 ± 3.9	−0.9 ± 5.2
cor	550 ± 73	−4.7 ± 7.1	−6.1 ± 11.4

Uncertainties are $\pm 2\sigma$. Abbreviations: hib = hibonite, cor = corundum.

similar to that of the hibonite. Both phases have ^{16}O-rich compositions, similar to some that have previously been reported for CM hibonite (*e.g.*, Fahey *et al.*, 1987; Ireland *et al.*, 1992). These results indicate that M98-8 formed in an ^{16}O-rich environment and, unlike many melilite-rich inclusions (Clayton *et al.*, 1977), did not partially re-equilibrate with an ^{16}O-poor vapor following crystallization.

DISCUSSION

Formation of the Inclusion

We now consider ways in which this inclusion could have formed: gas-to-solid condensation, or crystallization from (a) a stable, condensate liquid; (b) a metastable liquid; or (c) a liquid formed by melting and/or evaporation of hibonite.

In thermodynamic models of equilibrium condensation from a solar gas for total pressures $<10^{-2}$ atm, corundum is the first major condensate. At $P^{tot} = 10^{-3}$ atm, for example, corundum condenses at 1770 K and, with decreasing temperature, is predicted to react with the nebular gas to form hibonite at 1743 K, followed by condensation of perovskite at 1688 K (Yoneda and Grossman, 1995). At higher pressures ($\geq 10^{-2}$ atm), either hibonite, grossite, or liquid is the first condensate. With corundum grains enclosed in hibonite, and perovskite mostly occurring at the edge of the inclusion, the crystallization sequence consistent with the texture of M98-8 is the same as the equilibrium condensation sequence for a solar gas at low pressures. The rounded shapes of the corundum grains are consistent with the predicted corundum-hibonite reaction relationship, and the angular voids between hibonite grains also might be expected for an aggregate of condensate grains. For crystallization from a liquid, on the other hand, voids tend to be round and crystals tightly intergrown, with the shapes of late crystals conforming to the shapes of early crystals. These features are typically found in the relatively common hibonite-spinel spherules (*e.g.*, MacPherson *et al.*, 1983, 1984).

Simon *et al.* (1996) calculated solid/gas distribution coefficients, summarized in Fig. 7a, for REE and Y condensation into hibonite and perovskite from the volatilities of these elements and activity coefficients for their solid solution into those phases. The chondrite-normalized REE abundance

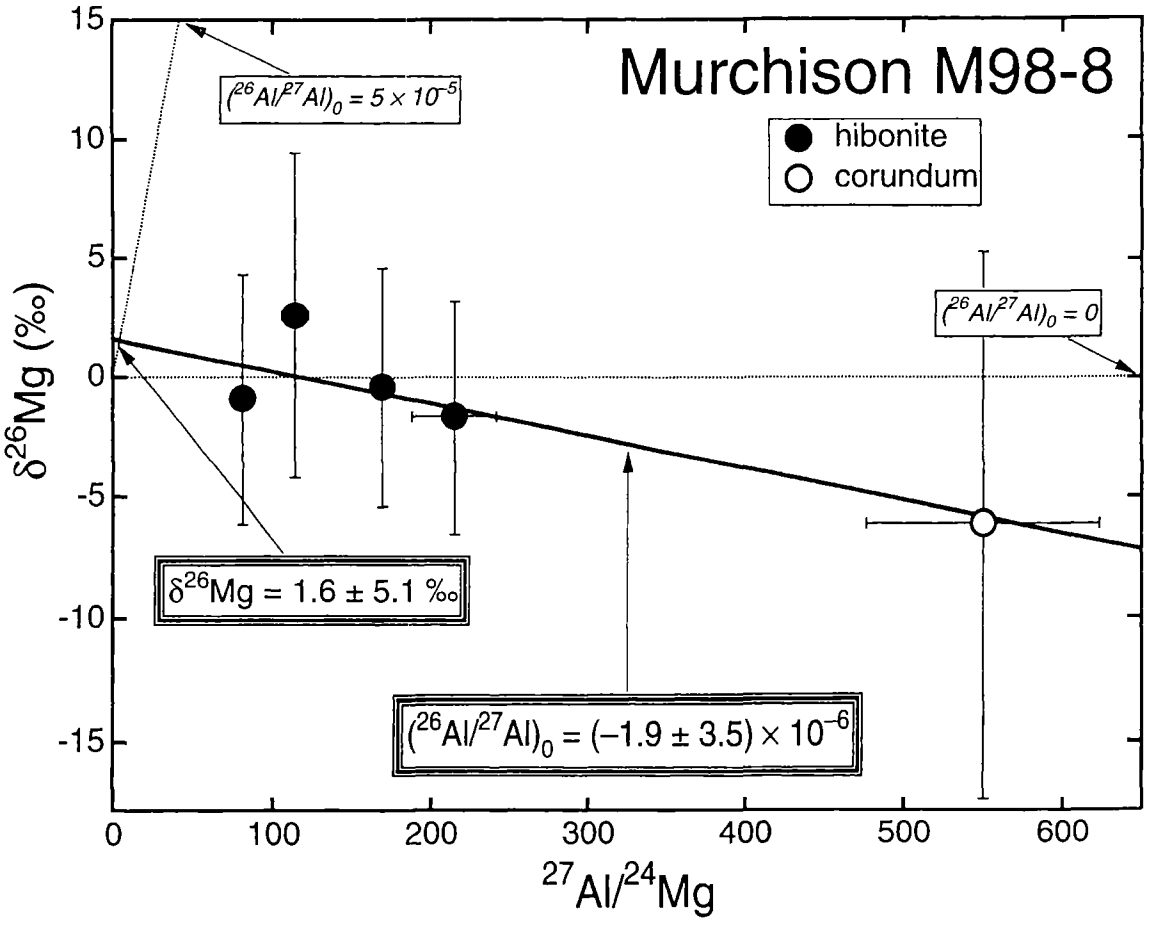

FIG. 6. $\delta^{26}Mg$, corrected for mass-fractionation, *vs.* $^{27}Al/^{24}Mg$ for hibonite and corundum in M98-8. There is no evidence for excess ^{26}Mg. A best-fit line through the data points has a *y*-intercept and a negative slope that are within error of 0. Lines for initial $^{26}Al/^{27}Al$ ratios of 0 and 5×10^{-5} are shown for reference. All uncertainties are $\pm 2\sigma$.

TABLE 5. Oxygen isotopic compositions of phases in M98-8.

	$\delta^{18}O$ (‰)	2σ mean (‰)	$\delta^{17}O$ (‰)	2σ mean (‰)	$\Delta^{17}O$ (‰)	2σ mean (‰)	^{16}O-excess (‰)	2σ mean (‰)
Spot 1	–55.8	4.3	–53.6	3.9	–24.6	3.1	51.2	6.5
Spot 2	–49.1	4.5	–47.4	4.2	–21.9	3.6	45.6	7.5
Spot 3	–54.5	6.1	–52.7	5.0	–24.3	4.9	50.6	10.3

Spots 1 and 2 are hibonite. Spot 3 is corundum + hibonite. The mixing proportions are not well determined. The deviation of the oxygen isotopic composition from the terrestrial fractionation line may be expressed by $\Delta^{17}O$, where: $\Delta^{17}O = \delta^{17}O - 0.52 \times \delta^{18}O$. Alternatively, the distance along the CAI-mixing line (Clayton *et al.*, 1977) can be expressed by the ^{16}O-excess (Clayton and Mayeda, 1983) given by the expression: $(0.52 \times \delta^{18}O - \delta^{17}O)/(1 - 0.52)$.

patterns of these phases in M98-8 are consistent with a condensation origin in that they qualitatively resemble these calculated solid/gas distribution coefficient patterns fairly closely while showing little similarity to the patterns of hibonite/liquid or perovskite/liquid distribution coefficients measured by Kennedy *et al.* (1994). As shown in Fig. 7a, for both hibonite and perovskite, the solid/gas distribution coefficients decrease from Lu through Sm, are fairly flat for the LREE, and are very low for Eu and Yb, in a pattern quite like that of the chondrite-normalized REE abundances in the perovskite-rich analysis spot (Fig. 5). The only mismatch is for Tm, which, assuming a chondritic source, should be depleted relative to Er and have a chondrite-normalized abundance similar to those of the LREE but, in the sample, is enriched relative to Er and the LREE. It

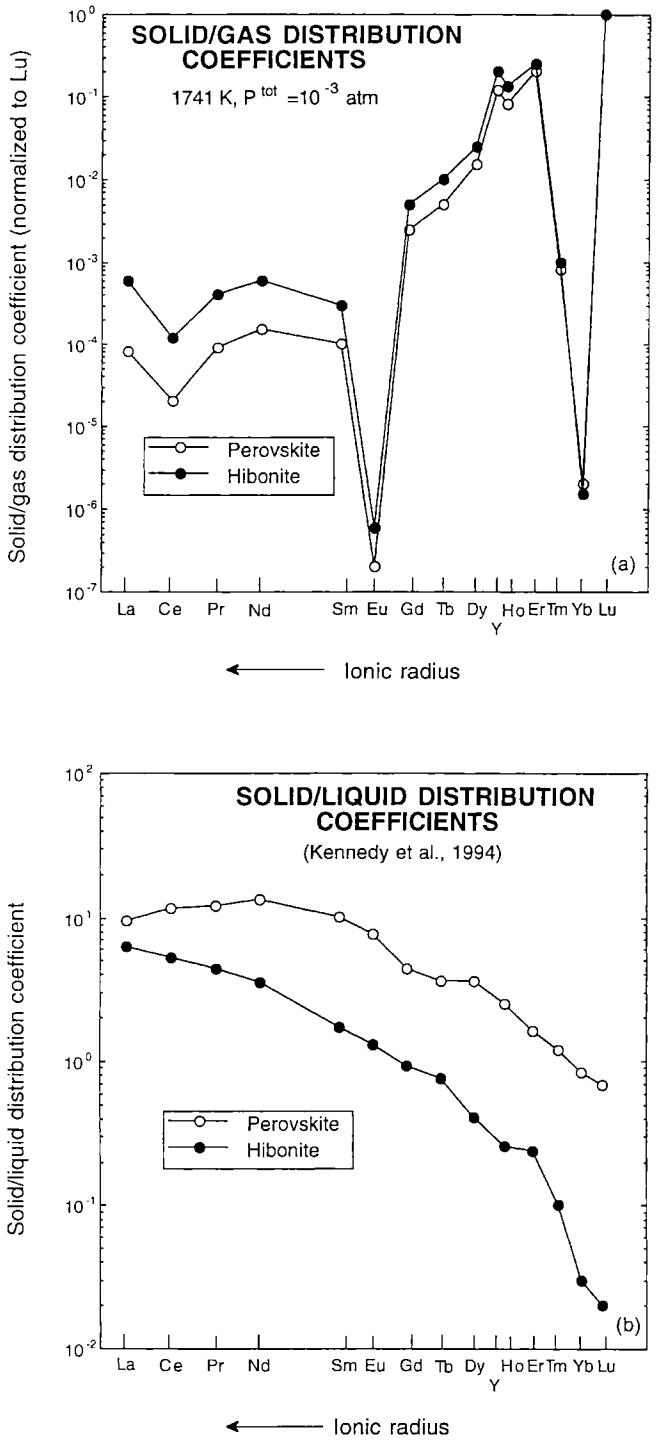

FIG. 7. (a) Solid/gas distribution coefficients, relative to that for Lu, calculated for condensation of REE from a solar gas into perovskite and hibonite at the conditions shown. After Simon *et al.* (1996). Note resemblance of these patterns to the observed hibonite-perovskite pattern (Fig. 5). (b) Solid/liquid distribution coefficients for perovskite and hibonite from the experiments of Kennedy *et al.* (1994).

is difficult to account for the observed Tm abundance for this spot. Oxidizing conditions can cause Tm enrichment in the solid, but such conditions would lead to negative Ce anomalies (Davis *et al.*, 1982), and these are not observed. In contrast with the solid/gas distribution coefficients and with the analyses of M98-8, the crystal/liquid distribution coefficients decrease from La through Lu (Fig. 7b).

From the bulk composition of M98-8, we know that if the inclusion had crystallized from a melt, perovskite could only crystallize late, after most or all of the hibonite. The results of Kennedy *et al.* (1994) show, however, that the light REE are compatible in hibonite, so perovskite that crystallized after hibonite should have relatively low LREE contents. We estimate that the perovskite-bearing analysis (#7, Table 3) sampled ~4 wt% perovskite. Assuming that the REE contents of the silicate are negligible and that the La content of the hibonite is ~18 × CI (Fig. 5), we calculate that the La content of the perovskite is >550 × CI. From the modal proportions of corundum, hibonite and perovskite in the inclusion, this leads to a bulk La content of ~25 × CI. Thus, the perovskite has a La content much greater than the bulk, which is inconsistent with prior crystallization of ~90% of a phase with a crystal/liquid distribution coefficient for La of ~6 (Kennedy *et al.*, 1994). The perovskite and the hibonite could not have crystallized from a common parental liquid.

There are additional problems with *any* model that includes a molten stage. From known phase relations (Berman, 1983) and the bulk Al_2O_3 content of M98-8 (over 88 wt%), we estimate that the inclusion would be completely molten only at temperatures >2140 K, but no condensed phases are stable in a solar gas at such temperatures at any P^{tot} < 10 atm (Yoneda and Grossman, 1995). For such an aluminous liquid to be stable at more reasonable total pressures, high dust/gas ratios and temperatures are required (*e.g.*, ~1000 × solar and 2400 K, respectively, for $P^{tot} = 10^{-3}$ atm; Yoneda and Grossman, 1995). Even if such conditions could be attained, Ca would continue to condense into the liquid, decreasing its Al_2O_3 content, during cooling so that, at the liquidus temperature, the liquid would be too CaO-rich to crystallize corundum, and would crystallize hibonite instead. Thus, in order to crystallize corundum from a stable liquid in the solar nebula, extraordinary *P–T* conditions would be required to form an extremely Al_2O_3-rich, CaO-poor liquid (note that these temperatures are much higher than those required for direct condensation of corundum), and the very early condensate liquid would have to be isolated from the nebular vapor and allowed to cool without further reaction with it. Furthermore, although this scenario would yield crystallization of corundum followed by hibonite, it probably would not produce the observed texture. Molten droplets typically cool by radiating heat from their surfaces, a process which, in this case, would probably form an outer zone of corundum enclosing a core of hibonite. Instead, in M98-8, we find small corundum grains enclosed within individual crystals of hibonite. Formation of M98-8 by crystallization of a stable molten droplet thus seems highly unlikely.

Metastable liquids could have existed in the nebula. Experiments (Nelson *et al.*, 1972; Keil *et al.*, 1973) have shown, however, that during rapid cooling and solidification of supercooled alumina droplets, nucleation and crystal growth are rapid, yielding spherulitic, cryptocrystalline textures quite unlike the texture of M98-8, with its massive, well-formed hibonite crystals. Even slow cooling of such droplets would be expected to yield quench textures. Calculations by Nelson *et al.* (1972) suggest that, in a completely molten droplet, the absence of crystal nucleii could permit significant degrees of undercooling even at much slower cooling rates than those used in their experiments, leading to rapid crystallization and therefore textures similar to those of quenched spherules. Slow cooling would also allow extensive evaporation from the melt, which leads to problems as described below. The features of M98-8 are not consistent with crystallization from a completely molten, stable or metastable condensate liquid.

Another way corundum can form is through the breakdown of hibonite. Hibonite melts incongruently to corundum + liquid. If a hibonite-rich inclusion were to be heated, melted, and partially evaporated, a corundum-bearing residue could result. This may have occurred during the formation of GR-1, a hibonite-corundum inclusion from Murchison first described by MacPherson *et al.* (1984). That inclusion has a basically concentric structure, with hibonite at the center enclosed in corundum, and hibonite also at the outer edge of the inclusion. MacPherson *et al.* (1984) noted that the core and rim hibonite had different Ti, Mg and Sc contents, and Hinton *et al.* (1988) found that they have contrasting trace element and isotopic compositions as well. As noted by these workers, the texture and the chemical data strongly suggest that this inclusion contains two generations of hibonite. What appears to have happened is that a hibonite-rich object was partially melted, leaving some residual hibonite; corundum formed, enclosing the relic hibonite in the interior, and all of the Ca evaporated from the liquid. The corundum later reacted with a Ca-bearing vapor to form the outer, REE-poor hibonite (Hinton *et al.*, 1988). Unlike that of M98-8, the texture of GR-1 suggests a hibonite–corundum–hibonite crystallization sequence, reflecting a complex thermal history.

Evaporation of hibonite was investigated experimentally by Floss *et al.* (1998), who rapidly heated, melted, and cooled hibonite samples in a vacuum furnace. They found that in all of their experiments, even one with only 6% mass loss, hibonite broke down completely, leading to run products consisting of corundum + glass ± thorianite ± a REE-rich phase. Unlike the GR-1 case, no relic hibonite was preserved, and no occurrences of corundum + hibonite were found. The occurrence of glass in these run products was probably due to the rapid cooling experienced by the liquid. If the melt had cooled slowly, avoiding formation of glass, it would have remained in the liquid state longer and presumably undergone fairly extensive evaporation of Mg and Ca. This would have resulted in strong isotopic mass fractionation, which is not observed, at least for Mg, in M98-8. In addition, evaporation of all oxides more volatile than Al_2O_3 would have lead to absence of hibonite.

In summary, there are serious problems with any model for the formation of M98-8 that includes a molten stage, relic phases or evaporation. Gas-to-solid condensation is the most straightforward way to account for the textural and chemical features of this sample.

Constraints on the Formation Conditions of M98-8

Given that M98-8 records a corundum–hibonite–perovskite (CHP) condensation sequence, thermodynamic calculations can be used to estimate under what combinations of temperature, pressure, and dust/gas ratio the sample could have formed. Increasing the dust/gas ratio increases the proportion of condensable elements in the system, and its effect is similar to that of increasing pressure. The model of Yoneda and Grossman (1995), summarized in Fig. 8, uses the thermodynamic data of Geiger *et al.* (1988) for grossite and hibonite and predicts a CHP sequence for condensation from a solar gas at pressures from ~5×10^{-3} (S. Yoneda, unpubl. data) through the lowest pressure modelled, 10^{-6} atm. Equilibrium condensation temperatures decrease with decreasing pressure. In the case of corundum, the temperature of the start of condensation, with no enrichment in dust relative to gas, ranges from 1770 K at 10^{-3} atm to 1571 K at 10^{-6} atm (Yoneda and Grossman, 1995). At pressures above the heavy dashed line in Fig. 8, corundum is not the first condensate according to these thermodynamic data.

The Geiger *et al.* (1988) data were preferred by Yoneda and Grossman (1995), but these data are not consistent with the liquid model of Berman (1983), which was used by Yoneda and Grossman (1995) for calculations in which liquid was predicted to be stable. Different data sets give different results. The Berman (1983) data for grossite and hibonite stabilize grossite relative to hibonite compared to the Geiger *et al.* (1988) data, predict grossite condensation before perovskite, and thus yield a corundum–hibonite–grossite sequence over much of the Geiger *et al.* (1988) CHP field in Fig. 8. As indicated by the horizontal lines in Fig. 8, the CHP sequence is restricted to pressures $<10^{-4}$ atm and CI dust/gas enrichments <10× solar (for $P^{tot} \geq 10^{-6}$ atm) when the Berman (1983) data are used, while use of the Geiger *et al.* (1988) data expands the field for the CHP condensation sequence to a much wider range of pressures and dust/gas ratios (vertical lines only), especially between 10^{-3} and 10^{-6} atm, which are generally considered the most likely pressures at which condensation took place in the solar nebula. Both data sets indicate that the CHP condensation sequence is favored by low total pressure and low dust/gas enrichment. Except for CH chondrites (*e.g.*, Grossman *et al.*, 1988; Brearley and Jones, 1998), grossite-bearing inclusions are very rare. Inclusions with hibonite and perovskite are much more common than hibonite-grossite

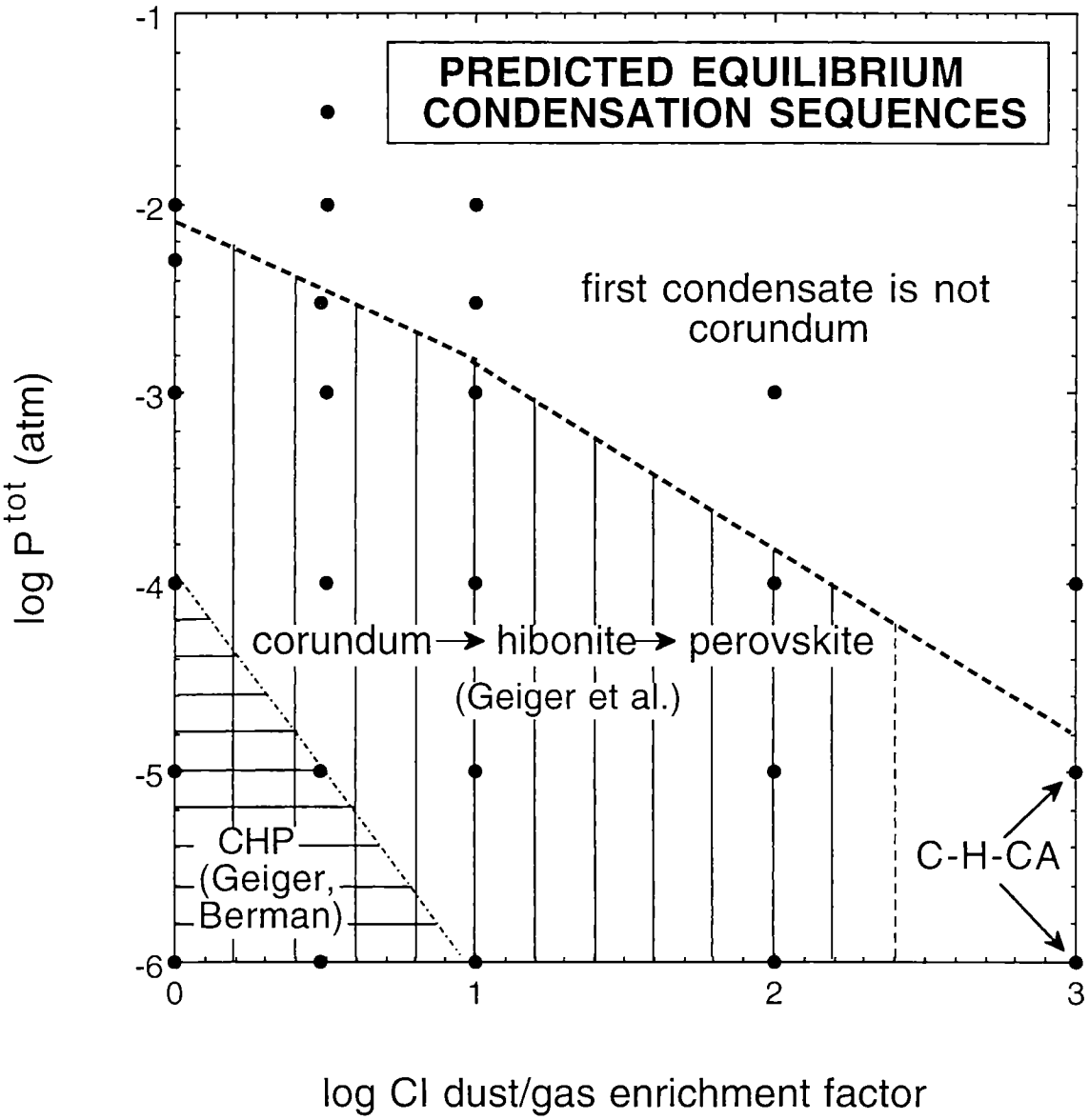

FIG. 8. A summary of the variation of equilibrium condensation sequence with total pressure (P^{tot}) and CI chondritic dust/gas enrichment relative to solar composition. Plotted points represent conditions for which thermodynamic calculations have been performed using data from Geiger *et al.* (1988) for hibonite and grossite. The range of conditions for which a corundum–hibonite–perovskite (CHP) condensation sequence is predicted using these data is represented by vertical lines; when data for hibonite and grossite from Berman (1983) are used, the CHP sequence is confined to the region with horizontal lines. The two points labelled C-H-CA have a corundum–hibonite–$CaAl_2O_4$ sequence. The extent of conditions for which this sequence is predicted has not been explored.

inclusions, so it is possible that the thermodynamic data of Berman (1983) overestimate the stability of grossite. Meteoritic hibonite contains Mg and Ti, however, and the degree to which these substitutions increase the stability of hibonite is not accounted for by either data set. Despite this limitation, we can say that if the Berman (1983) data are correct, and if the corundum-hibonite-grossite inclusion reported by Krot *et al.* (2001) is a condensate, then it could have formed at higher P^{tot} and/or higher dust/gas enrichment than M98-8.

Corundum-Bearing Inclusions: Implications for Distribution of Aluminum-26 in the Early Solar Nebula

Corundum-bearing inclusions are very rare, probably because if they were not removed from the nebular gas soon after they formed, the corundum would have continued to react with the gas to form hibonite. In addition to M98-8 and GR-1, two other corundum-bearing samples have been analyzed by ion probe. They both may be condensates from the early solar nebula but do not have many features in common. Murchison

sample BB-5 (Bar-Matthews *et al.*, 1982) has a corundum-rich core enclosed in hibonite in a texture that has small void spaces and is more compact than that of M98-8. Like M98-8, BB-5 has chondrite-normalized heavy REE abundances > light REE and no excess ^{26}Mg, indicating that the sample did not contain live ^{26}Al when it formed. Murray sample F5 has a group II REE pattern, and it contains excess ^{26}Mg consistent with *in situ* decay of ^{26}Al and an initial ^{26}Al/^{27}Al ratio of $(4.1 \pm 0.2) \times 10^{-5}$ (Fahey, 1988). Of the three corundum-bearing inclusions that may be primary condensates, two (BB-5 and M98-8) did not contain live ^{26}Al when they formed, although many other, less refractory (*e.g.*, melilite-bearing) CAIs did (MacPherson *et al.*, 1995).

Because evidence for ^{26}Al is found in many, but not all, refractory inclusions, the origin of this radionuclide and its significance for constraining the timescales of formation of CAIs are controversial. From its short half-life (7.3×10^5 years) we know that ^{26}Al must have entered CAIs soon (*i.e.*, not more than a few million years) after its synthesis. This relatively short timescale has led to two competing suggestions: either ^{26}Al formed in the solar system by irradiation of CAIs (or their precursors) by solar energetic particles, as in the X-wind model (*e.g.*, Shu *et al.*, 1997; Lee *et al.*, 1998; Gounelle *et al.*, 2001), or it was added as a spike of freshly synthesized nuclides from a single stellar source (*e.g.*, Lee *et al.*, 1977; Sahijpal and Goswami, 1998; Goswami *et al.*, 2001). In its favor, the X-wind model provides a mechanism for removal of CAIs from their formation region, which is necessary for the preservation of high-temperature assemblages. Also, that there was some radionuclide production by solar particle irradiation is evident from the existence of live ^{10}Be in CAIs (McKeegan *et al.*, 2000), as all Be is destroyed in stellar interiors and ^{10}Be can only be made by spallation, either in the interstellar medium, where the galactic cosmic ray flux is low, or by solar flares near the Sun. Serious problems with an analogous origin for ^{26}Al, and evidence for seeding of the solar nebula by radioactive stellar debris, however, result from the observation that in hibonite, ^{26}Al almost always occurs with an even shorter-lived ($t_{1/2} \approx 10^5$ years) radionuclide, ^{41}Ca (Sahijpal and Goswami, 1998; Sahijpal *et al.*, 1998, 2000). Calculations using measured and calculated nuclear cross-sections show that particle irradiation cannot simultaneously produce the correct initial ^{26}Al and ^{41}Ca abundances from the same target material (Shu *et al.*, 1997; Sahijpal and Goswami, 1998; Lee *et al.*, 1998; Sahijpal *et al.*, 2000; Goswami *et al.*, 2001).

This problem led proponents of irradiation (Shu *et al.*, 1997, 2001; Gounelle *et al.*, 2001) to suggest that ^{26}Al was made in thick (~3 mm), Ca-free ferromagnesian mantles that enclosed CAIs and provided sufficient shielding to yield the observed initial ^{26}Al without overproduction of ^{41}Ca. The models for mantle formation, however, ignore major petrologic constraints. Shu *et al.* (2001) invoke formation of the mantles by melting of chondritic dust and generation of immiscible liquids, but experimentally determined phase equilibria show that chondritic melts do not give rise to immiscible liquids. Gounelle *et al.* (2001) likened the mantle-forming process to the "zone refining" technique used for purifying metal. For this to work on proto-CAIs, a heat pulse would have to move from the outside of the CAIs inward, driving the residual melt toward the cores, but during heating by solar flares, as envisioned by Gounelle *et al.* (2001), the insides of the objects will be no hotter than the outsides. This would yield objects with forsteritic interiors and Ca-, Al-, Si-rich exteriors containing no corundum, hibonite or melilite, because partial melting of chondritic matter cannot produce a residue of CAI composition. The accretionary rims that are observed around CAIs do not meet the requirements of the X-wind model. The rims reach 3 mm in thickness only where they fill embayments in the host CAIs, and they are not Ca-free (MacPherson *et al.*, 1985).

Even if suitable ferromagnesian mantles did exist, it would be very difficult, perhaps impossible, to transport ^{26}Al from them into CAIs in a way that yields not only a dominant initial ^{26}Al/^{27}Al ratio among many CAIs, but also accounts for the fact that phases in CAIs fall on Al-Mg isochrons. The existence of isochrons requires that the ^{26}Al/^{27}Al ratio was uniform throughout each CAI as an initial condition, further requiring that, when ^{26}Al was incorporated, the constituent minerals of such CAIs equilibrated with a common fluid phase, probably implying that the CAIs were molten. The Gounelle *et al.* (2001) model calls for entry of ^{26}Al into the nebular gas by vaporization of the ^{26}Al-bearing ferromagnesian mantles without vaporization of the CAIs themselves. Actually, the ^{26}Al would probably not evaporate, but would stay in the proto-CAIs even as they underwent the nearly complete melting implied by the isochrons. Melting of the entire proto-CAI + mantle assemblage after ^{26}Al production would not be allowed, because this would result in a homogeneous droplet much more Mg- and Si-rich than observed CAIs. Formation of CAIs as evaporative residues of compositions this rich (*i.e.*, near-chondritic) in Mg and Si would produce much larger Mg and Si isotopic mass-fractionations than are observed in CAIs. It is highly unlikely, however, that the ferromagnesian mantles could be heated and evaporated without some dissolution of them into the molten CAI cores, also requiring more extensive Mg and Si evaporation and isotopic fractionation than are indicated by the isotopic compositions of CAIs. Finally, in another unlikely scenario, at very particular temperatures at low nebular pressures, solid-to-vapor evaporation of mantles could occur while solid CAI cores remain intact. A subsequent melting event would then be required to permit incorporation of ^{26}Al uniformly into the CAIs.

In light of the problems of coproduction of the observed abundances of radionuclides by energetic particle irradiation, arguments for a stellar source for ^{26}Al and ^{41}Ca are discussed by Sahijpal and Goswami (1998) and Sahijpal *et al.* (1998, 2000). Models must account for the uniformity of initial abundances of ^{26}Al and ^{41}Ca and for the formation of hibonite with both and without both of these radionuclides. Three possibilities for the formation of ^{26}Al-free inclusions, such as M98-8, were considered by Sahijpal and Goswami (1998) and

Sahijpal *et al.* (2000). They are (1) formation before injection of ^{26}Al into the nebula was completed; (2) formation after ^{26}Al decay; and (3) heterogeneous distribution of ^{26}Al in the solar nebula. Their analyses and data from the literature (*e.g.*, Clayton *et al.*, 1988; MacPherson *et al.*, 1995) show that inclusions that did not incorporate ^{26}Al also did not incorporate ^{41}Ca and exhibit large isotopic anomalies of nucleosynthetic origin in ^{48}Ca and ^{50}Ti relative to most CAIs. They interpreted these features as primary nucleosynthetic signatures. In rejecting the heterogeneous distribution model, these workers noted the conclusion by MacPherson *et al.* (1995) that Al isotopic heterogeneity appears to have been minor among CAI precursors, which were strongly dominated by materials with initial ^{26}Al/^{27}Al ratios of 5×10^{-5}. This interpretation of the data is consistent with the nebular evolution models of Foster and Boss (1997), which predict limited heterogeneity of ^{26}Al due to steady (as opposed to episodic) injection of live radionuclides during the collapse of the solar nebula. Formation of ^{26}Al-free inclusions after decay of the radionuclide is also not favored, because this would require formation of ^{26}Al-bearing inclusions early, storage of these inclusions in the nebula for several million years, then formation of even more highly refractory inclusions, and incorporation of ^{26}Al-free and ^{26}Al-bearing inclusions into the same parent bodies. Assuming a stellar source for the radionuclides and that the travel time between the source and the protosolar cloud was negligible, Sahijpal and Goswami (1998) and Sahijpal *et al.* (2000) concluded that ^{26}Al-free hibonite grains and hibonite-, corundum-rich refractory inclusions formed very early in the history of the solar system, during a presumed about (2–6) $\times$ 10^5 year interval between impact of the stellar shock front that triggered the collapse of the solar nebula and the injection of live radionuclides (^{26}Al and ^{41}Ca) into the CAI-forming region. This model has the advantages of (a) explaining the correlation between ^{26}Al and ^{41}Ca abundances in CAIs and (b) not invoking a several million-year gap between generations of CAIs.

The present sample, M98-8, did not contain live ^{26}Al when it formed, and within the context of the Sahijpal *et al.* (2000) model it would therefore correspond to a condensate assemblage from the earliest phases of the solar nebula. Sample F5 is a hibonite-rich sample that did contain ^{26}Al when it formed, and it has a group II REE pattern (Fahey, 1988), which is indicative of prior volatility-related fractionation of its precursors. This suggests that its formation occurred somewhat later.

Formation of Oxygen-16-Rich Inclusions

Ion probe analyses show that the most refractory phases of CAIs tend to be the most ^{16}O-rich, with $\delta^{18}O \approx \delta^{17}O$ and typically between –40 and –50‰ (*e.g.*, Ireland *et al.*, 1992). These are thought to represent the primary isotopic compositions of the phases, and therefore that of the early nebular vapor, while phases with isotopic compositions closer to normal are thought to have obtained their compositions through reaction with a relatively ^{16}O-poor gas (Clayton *et al.*, 1977). Although ^{16}O is made in supernovae, as is ^{26}Al, the ^{16}O enrichments are not correlated with ^{26}Al and ^{41}Ca contents. Hibonite tends to be ^{16}O-rich, about –50‰, whether or not it contained live ^{26}Al when it formed (Fahey *et al.*, 1987). This implies that ^{16}O was not injected into the nebula along with the short-lived nuclides. It is not known how the nebular gas became ^{16}O-rich. Some workers favor evaporation of ^{16}O-rich dust to form ^{16}O-rich gas (Scott and Krot, 2001; Cassen, 2001). Their models, based on observed compositions of phases in CAIs and ^{16}O-rich endmembers assumed to have $\delta^{17}O = -50‰$, suggest that ^{16}O-rich phases in CAIs formed from a vapor enriched in dust by a factor of ~30 relative to solar composition. A corundum–hibonite–perovskite condensation sequence would still be possible at this degree of dust enrichment at low P^{tot} (Fig. 8), but for $P^{tot} \approx 10^{-3}$ atm or higher, corundum would not be the first condensate and condensation of liquid would be likely (Yoneda and Grossman, 1995; Ebel and Grossman, 2000). If dust enrichment is required to produce ^{16}O-rich minerals, this would place an upper limit on the range of pressures at which inclusions thought to be gas-to-solid condensates could have formed. Another way to produce an ^{16}O-rich gas may be by non-mass-dependent isotopic fractionation during gas-phase chemical reactions (*e.g.*, Thiemens, 1999), but this process has not been shown to work for either SiO or CO, the dominant oxygen-containing molecules in a solar gas.

CONCLUSIONS

M98-8 consists of corundum, hibonite, and perovskite, the first three condensate minerals predicted to form by equilibrium condensation from the solar nebula under certain conditions. From petrographic observations, chemical and isotopic data, and the inability of any model that includes a molten stage, relic grains or evaporation to account for the features of this inclusion, we conclude that it is a primary condensate from an ^{16}O-rich gas in the early solar nebula. Thermodynamic condensation calculations show that a corundum–hibonite–perovskite sequence is possible under a fairly wide range of total pressures $\leq 5 \times 10^{-3}$ atm, including those typically favored for refractory inclusion formation. The lower the pressure, the higher the permissible dust/gas enrichment, up to between 100 and 1000 $\times$ solar for $P^{tot} = 10^{-6}$ atm. The sample did not contain live ^{26}Al when it formed, which is consistent with the Sahijpal and Goswami (1998) model for the injection of ^{26}Al into the solar nebula, which suggests that ^{26}Al-free refractory inclusions are among the first solids formed in the solar system. If this model is correct, then M98-8 formed within ~6×10^5 years of the beginning of the collapse of the protosolar cloud.

Acknowledgments–We wish to thank R. Elsenheimer for performing the disaggregation and finding the sample, and D. S. Ebel and S. Yoneda for condensation calculations. Reviews by A. N. Krot and J. N.

Goswami led to improvements in the text. This work was supported by the National Aeronautics and Space Administration (NASA) through grants NAG5-4476 (L. G.), NAG5-9510 (A. M. D.), and NAG5-9798 (K. D. M.) and funding is gratefully acknowledged. The UCLA ion microprobe laboratory is partially supported by a grant from the National Science Foundation Instrumentation and Facilities program.

Editorial handling: I. C. Lyon

REFERENCES

BAR-MATTHEWS M., HUTCHEON I. D., MACPHERSON G. J. AND GROSSMAN L. (1982) A corundum-rich inclusion in the Murchison meteorite. *Geochim. Cosmochim. Acta* **46**, 31–41.

BECKETT J. R., SIMON S. B. AND STOLPER E. (2000) The partitioning of Na between melilite and liquid: Part II. Application to type B inclusions from carbonaceous chondrites. *Geochim. Cosmochim. Acta* **64**, 2519–2534.

BERMAN R. G. (1983) A thermodynamic model for multicomponent melts, with application to the system CaO-MgO-Al_2O_3-SiO_2. Ph.D. dissertation, Univ. British Columbia, Vancouver, British Columbia, Canada. 149 pp.

BREARLEY A. J. AND JONES R. H. (1998) Chondritic meteorites. In *Planetary Materials* (ed. J. J. Papike), pp. 3-1 to 3-398. *Revs. Mineral.* **36**, Mineral. Soc. Amer., Washington, D.C., USA.

CASSEN P. (2001) Nebular thermal evolution and the properties of primitive planetary materials. *Meteorit. Planet. Sci.* **36**, 671–700.

CLAYTON R. N. AND MAYEDA T. K. (1983) Oxygen isotopes in eucrites, shergottites, nakhlites, and chassignites. *Earth Planet. Sci. Lett.* **62**, 1–6.

CLAYTON R. N., ONUMA N., GROSSMAN L. AND MAYEDA T. K. (1977) Distribution of the pre-solar component in Allende and other carbonaceous chondrites. *Earth Planet. Sci. Lett.* **34**, 209–224.

CLAYTON R. N., HINTON R. W. AND DAVIS A. M. (1988) Isotopic variations in the rock-forming elements in meteorites. *Phil. Trans. Royal Soc. London* **A325**, 483–501.

DAVIS A. M., TANAKA T., GROSSMAN L., LEE T. AND WASSERBURG G. J. (1982) Chemical composition of HAL, an isotopically-unusual Allende inclusion. *Geochim. Cosmochim. Acta* **46**, 1627–1651.

EBEL D. S. AND GROSSMAN L. (2000) Condensation in dust-enriched systems. *Geochim. Cosmochim. Acta* **64**, 339–366.

FAHEY A. J. (1988) Ion microprobe measurements of Mg, Ca, Ti and Fe isotopic ratios and trace element abundances in hibonite-bearing inclusions from primitive meteorites. Ph. D. dissertation, Washington Univ., St. Louis, Missouri, USA. 232 pp.

FAHEY A. J., GOSWAMI J. N., MCKEEGAN K. D. AND ZINNER E. K. (1987) ^{16}O excesses in Murchison and Murray hibonites: A case against a late supernova injection origin of isotopic anomalies in O, Mg, Ca and Ti. *Astrophys. J. Lett.* **323**, L91–L95.

FLOSS C., EL GORESY A., ZINNER E., PALME H., WECKWERTH G. AND RAMMENSEE W. (1998) Corundum-bearing residues produced through the evaporation of natural and synthetic hibonite. *Meteorit. Planet. Sci.* **33**, 191–206.

FOSTER P. N. AND BOSS A. P. (1997) Injection of radioactive nuclides from the stellar source that triggered the collapse of the presolar nebula. *Astrophys. J.* **489**, 346–357.

GEIGER C. A., KLEPPA O. J., MYSEN B. O., LATTIMER J. M. AND GROSSMAN L. (1988) Enthalpies of formation of $CaAl_4O_7$ and $CaAl_{12}O_{19}$ (hibonite) by high temperature, alkali borate solution calorimetry. *Geochim. Cosmochim. Acta* **52**, 1729–1736.

GOSWAMI J. N., MARHAS K. K. AND SAHIJPAL S. (2001) Did solar energetic particles produce the short-lived nuclides present in the early solar system? *Astrophys. J.* **549**, 1151–1159.

GOUNELLE M., SHU F. H., SHANG H., GLASSGOLD A. E., REHM K. E. AND LEE T. (2001) Extinct radioactivities and protosolar cosmic rays: Self-shielding and light elements. *Astrophys. J.* **548**, 1051–1070.

GROSSMAN J. N., RUBIN A. E. AND MACPHERSON G. J. (1988) ALH 85085: A unique volatile-poor carbonaceous chondrite with implications for nebular fractionation processes. *Earth Planet. Sci. Lett.* **91**, 33–54.

GROSSMAN L., EBEL D. S., SIMON S. B., DAVIS A. M., RICHTER F. M. AND PARSAD N. (2000) Major element chemical and isotopic compositions of refractory inclusions in C3 chondrites: The separate roles of condensation and evaporation. *Geochim. Cosmochim. Acta* **64**, 2879–2894.

HINTON R. W., DAVIS A. M., SCATENA-WACHEL D. E., GROSSMAN L. AND DRAUS R. J. (1988) A chemical and isotopic study of hibonite-rich refractory inclusions in primitive meteorites. *Geochim. Cosmochim. Acta* **52**, 2573–2598.

IRELAND T. R. (1988) Correlated morphological, chemical, and isotopic characteristics of hibonites from the Murchison carbonaceous chondrite. *Geochim. Cosmochim. Acta* **52**, 2827–2839.

IRELAND T. R., FAHEY A. J. AND ZINNER E. K. (1988) Trace-element abundances in hibonites from the Murchison carbonaceous chondrite: Constraints on high-temperature processes in the solar nebula. *Geochim. Cosmochim. Acta* **52**, 2841–2854.

IRELAND T. R., FAHEY A. J. AND ZINNER E. K. (1991) Hibonite-bearing microspherules: A new type of refractory inclusions with large isotopic anomalies. *Geochim. Cosmochim. Acta* **55**, 367–379.

IRELAND T. R., ZINNER E. K., FAHEY A. J. AND ESAT T. M. (1992) Evidence for distillation in the formation of HAL and related hibonite inclusions. *Geochim. Cosmochim. Acta* **56**, 2503–2520.

KEIL K., PRINZ M., PLANNER H. N., SKAGGS S. R., DOWTY E., NELSON L. S., RICHARDSON N. L. AND BLANDER M. (1973) A qualitative comparison of textures in lunar chondrules and CO_2 laser-formed synthetic chondrule-like spherules. *UNM Inst. Meteoritics Spec. Pub.* **7**, 16 pp.

KENNEDY A. K., LOFGREN G. E. AND WASSERBURG G. J. (1994) Trace-element partition coefficients for perovskite and hibonite in meteorite compositions. *Chem. Geol.* **117**, 379–390.

KROT A. N., HUSS G. R. AND HUTCHEON I. D. (2001) Corundum-hibonite refractory inclusions from Adelaide: Condensation or crystallization from melt? (abstract). *Meteorit. Planet. Sci.* **36 (Suppl.)**, A105.

LEE T., PAPANASTASSIOU D. A. AND WASSERBURG G. J. (1977) Aluminum-26 in the early solar system: Fossil or fuel? *Astrophys. J.* **211**, L107–L110.

LEE T., SHU F. H., SHANG H., GLASSGOLD A. E. AND REHM K. E. (1998) Protostellar cosmic rays and extinct radioactivities in meteorites. *Astrophys. J.* **506**, 898–912.

MACPHERSON G. J. AND DAVIS A. M. (1993) A petrologic and ion microprobe study of a Vigarano type B refractory inclusion: Evolution by multiple stages of alteration and melting. *Geochim. Cosmochim. Acta* **57**, 231–243.

MACPHERSON G. J. AND DAVIS A. M. (1994) Refractory inclusions in the prototypical CM chondrite, Mighei. *Geochim. Cosmochim. Acta* **58**, 5599–5625.

MACPHERSON G. J., BAR-MATTHEWS M., TANAKA T., OLSEN E. AND GROSSMAN L. (1980) Refractory inclusions in Murchison: Recovery and mineralogical description (abstract). *Lunar Planet. Sci.* **11**, 660–662.

MACPHERSON G. J., BAR-MATTHEWS M., TANAKA T., OLSEN E. AND GROSSMAN L. (1983) Refractory inclusions in the Murchison meteorite. *Geochim. Cosmochim. Acta* **47**, 823–839.

MACPHERSON G. J., GROSSMAN L., HASHIMOTO A., BAR-MATTHEWS M. AND TANAKA T. (1984) Petrographic studies of refractory inclusions from the Murchison meteorite. *Proc. Lunar Planet. Sci. Conf.* **15th**, *J. Geophys. Res.* **89**, C299–C312.

MACPHERSON G. J., HASHIMOTO A. AND GROSSMAN L. (1985) Accretionary rims on inclusions in the Allende meteorite. *Geochim. Cosmochim. Acta* **49**, 2267–2279.

MACPHERSON G. J., DAVIS A. M. AND ZINNER E. K. (1995) The distribution of aluminum-26 in the early solar system—A reappraisal. *Meteoritics* **30**, 365–386.

MCKEEGAN K. D., CHAUSSIDON M. AND ROBERT F. (2000) Incorporation of short-lived ^{10}Be in a calcium-aluminum-rich inclusion from the Allende meteorite. *Science* **289**, 1334–1337.

NELSON L. S., BLANDER M., SKAGGS S. R. AND KEIL K. (1972) Use of a CO_2 laser to prepare chondrule-like spherules from supercooled molten oxide and silicate droplets. *Earth Planet. Sci. Lett.* **14**, 338–344.

POUCHOU J. L. AND PICHOIR F. (1984) A new model for quantitative x-ray microanalysis. Part I: Application to the analysis of homogeneous samples. *Rech. Aerosp.* **3**, 13–38.

RUSSELL S. S., DAVIS A. M., MACPHERSON G. J., GUAN Y. AND HUSS G. R. (2000) Refractory inclusions from the ungrouped carbonaceous chondrites MAC 87300 and MAC 88107. *Meteorit. Planet. Sci.* **35**, 1051–1066.

SAHIJPAL S. AND GOSWAMI J. N. (1998) Refractory phases in primitive meteorites devoid of ^{26}Al and ^{41}Ca: Representative samples of first solar system solids? *Astrophys. J.* **509**, L137–L140.

SAHIJPAL S., GOSWAMI J. N., DAVIS A. M., GROSSMAN L. AND LEWIS R. S. (1998) A stellar origin for the short-lived nuclides in the early solar system. *Nature* **391**, 559–561.

SAHIJPAL S., GOSWAMI J. N. AND DAVIS A. M. (2000) K, Mg, Ti and Ca isotopic compositions and refractory trace element abundances in hibonites from CM and CV meteorites: Implications for early solar system processes. *Geochim. Cosmochim. Acta* **64**, 1989–2005.

SCOTT E. R. D. AND KROT A. N. (2001) Oxygen-isotopic compositions and origins of calcium-aluminum-rich inclusions and chondrules. *Meteorit. Planet. Sci.* **36**, 1307–1319.

SHU F. H., SHANG H., GLASSGOLD A. E. AND LEE T. (1997) X-rays and fluctuating X-wind from protostars. *Science* **277**, 1475–1479.

SHU F. H., SHANG H., GOUNELLE M., GLASSGOLD A. E. AND LEE T. (2001) The origin of chondrules and refractory inclusions in chondritic meteorites. *Astrophys. J.* **548**, 1029–1050.

SIMON S. B., GROSSMAN L. AND DAVIS A. M. (1991) Fassaite composition trends during crystallization of Allende type B refractory inclusion melts. *Geochim. Cosmochim. Acta* **55**, 2635–2655.

SIMON S. B., DAVIS A. M. AND GROSSMAN L. (1996) A unique ultrarefractory inclusion from the Murchison meteorite. *Meteorit. Planet. Sci.* **31**, 106–115.

SIMON S. B., GROSSMAN L. AND ELSENHEIMER R. (2000a) First rock from the Sun: A corundum-hibonite condensate from Murchison (abstract). *Meteorit. Planet. Sci.* **35 (Suppl.)**, A148.

SIMON S. B., MCKEEGAN K. D., EBEL D. S. AND GROSSMAN L. (2000b) Complexly zoned chromium-aluminum spinel found *in situ* in the Allende meteorite. *Meteorit. Planet. Sci.* **35**, 215–227.

THIEMENS M. H. (1999) Mass-independent isotope effects in planetary atmospheres and the early solar system. *Science* **283**, 341–345.

YONEDA S. AND GROSSMAN L. (1995) Condensation of CaO-MgO-Al_2O_3-SiO_2 liquids from cosmic gases. *Geochim. Cosmochim. Acta* **59**, 3413–3444.